

Tensor renormalization group in bosonic field theory

Manuel Campos, Germán Sierra, and Esperanza López

Instituto de Física Teórica UAM/CSIC, C/Nicolás Cabrera 13-15, Cantoblanco, 28049 Madrid, Spain



(Received 28 February 2019; revised manuscript received 2 October 2019; published 6 November 2019)

We compute the partition function of a massive free boson in a square lattice using a tensor network algorithm. We introduce a singular value decomposition of continuous matrices that leads to very accurate numerical results. It shows the emergence of a corner double line fixed-point structure. In the massless limit, we reproduce the results of conformal field theory including a precise value of the central charge.

DOI: [10.1103/PhysRevB.100.195106](https://doi.org/10.1103/PhysRevB.100.195106)

I. INTRODUCTION

Tensor networks (TNs) have become in recent years a standard technique to study a wide variety of problems in condensed-matter physics, statistical mechanics, quantum-field theory, and other areas of physics [1,2]. In quantum lattice systems, TNs provide variational ansätze for many-body wave functions denoted tensor network states (TNSs). Well-known examples of TNSs are matrix product states (MPSs) for one-dimensional (1D) systems [3–8] that underlie the density-matrix renormalization-group (DMRG) method [9–11], projected entangled pairs states that is a two-dimensional (2D) version of MPSs [12,13], multiscale entanglement renormalization ansatz (MERA) [14–16], etc. The use of TNSs has also made it possible to classify the symmetry-protected phases in 1D, explore the topological phases of matter in 2D [17–19], and provide simple versions of holography in the anti-de Sitter/conformal field theory (AdS/CFT) correspondence [20–25].

In classical spin systems, the DMRG techniques were applied to compute the partition function [26]. Later on, the method was improved expressing the partition function and correlations using four-index tensors [27]. An important step was made by Levin and Nave who proposed the tensor renormalization group (TRG) [28] where the Kadanoff-Wilson blocking method is improved by implementing entanglement techniques in the truncation procedure [29,30]. However, the TRG does not fully succeed in removing the short-range entanglement. For noncritical systems, the TRG converges towards nontrivial tensors with a *corner double line* (CDL) structure [31]. This difficulty was solved by implementing techniques first developed for MERA [32,33].

The aim of this paper is to explore the application of real-space tensor network techniques to study quantum-field theories. Our motivation is to revisit quantum-field theory, and, in particular, renormalization-group issues from a framework naturally adapted to capture the role played by entanglement. A systematic study of quantum-field theories is only available in the perturbative framework where the free theory is the starting point. Hence, as a first step towards more interesting cases, we efficiently adapt the TRG protocol to evaluate the partition function of a free boson. Like in the

ordinary TRG, a CDL-type infrared fixed point emerges at the expected length scale. In the conformal limit, we obtain a competitive estimation for the value of the central charge. Our implementation of the TRG is based on the simple rules of Gaussian integration, and hence, we name it Gaussian TRG (gTRG).

The paper is structured as follows. Section II explains the model we are going to study. Section III presents the renormalization-group algorithm, which is the central point of this paper. Results obtained using the algorithm are shown in Sec. IV, and they are compared with the analytical computations. Section V studies the renormalization flow, paying special attention to the emerging CDL structure. Finally, in Sec. VI, we present our conclusions and point out future directions of research.

II. THE MODEL

We will consider a free scalar of mass m in two dimensions. Continuous versions of tensor networks have been proposed for the study of quantum-field theories [34–39]. However, they are not yet developed to the extent ordinary tensor networks are, and we will not pursue them here. In the following, space-time will be discretized whereas field variables retain their continuous character. This choice breaks symmetries, such as translation and rotation, but they can be recovered in the continuum limit. Space-time will be represented by a square lattice with periodic boundary conditions. At each site (i, j) of the lattice lives a variable $\phi_{ij} \in \mathbb{R}$. The Euclidean partition function is

$$Z = \int \prod_{ij} d\phi_{ij} \exp \left\{ -\frac{1}{2} \sum_{ij} [(\phi_{ij} - \phi_{i+1j})^2 + (\phi_{ij} - \phi_{ij+1})^2 + m^2 \phi_{ij}^2] \right\}, \quad (1)$$

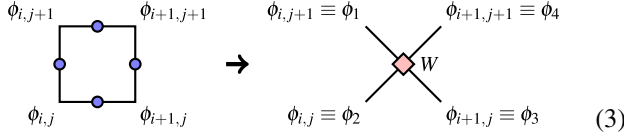
where m is measured in lattice units.

The interactions on the lattice described by (1) are pairwise between the fields at neighbor sites. It is convenient to change to a vertex model where the fields live on the edges and the interactions take place at the lattice sites. On the dual tilted

lattice, we define the statistical weights,

$$W(\phi_i) = \exp \left\{ -\frac{1}{2} \sum_{i=1}^4 \left[(\phi_i - \phi_{i+1})^2 + \frac{m^2}{2} \phi_i^2 \right] \right\}, \quad (2)$$

with the fields relabeled as follows:



$$\begin{array}{ccc} \phi_{i,j+1} & \phi_{i+1,j+1} & \phi_{i,j+1} \equiv \phi_1 \\ \phi_{i,j} & \phi_{i+1,j} & \phi_{i,j} \equiv \phi_2 \end{array} \quad \rightarrow \quad \begin{array}{ccc} & \phi_{i+1,j+1} \equiv \phi_4 & \\ & \diagdown & \diagup \\ & \phi_{i+1,j} \equiv \phi_3 & \\ & \diagup & \diagdown \\ & \phi_{i,j} \equiv \phi_2 & \end{array} \quad (3)$$

We have shaded the interaction vertices for clarity.

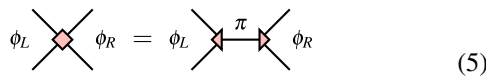
III. GAUSSIAN TRG

We will implement a TRG protocol to reduce iteratively the number of degrees of freedom. The basic tool used in systems with a finite number of degrees of freedom is the singular value decomposition (SVD) of the network tensors. Any finite rank matrix can be decomposed as $M = USV^\dagger$, where U and V are unitary matrices and S is diagonal with non-negative entries. The latter result also holds for compact operators acting on Hilbert spaces of continuous functions. This result has been used to implement the standard TRG approach to a ϕ^4 -boson field theory [40]. In this reference, the two-body interaction is truncated to a finite-dimensional space in order to verify the Monte Carlo scaling relation for the expectation value of the boson field at criticality. Here, we will not follow this approach but one that is inspired from standard field-theory techniques. Indeed, at each step of the coarse-graining procedure, we will impose that the statistical weights should remain Gaussian for continuous fields.

We will allow several fields to live at each lattice edge. For simplicity, we still denote them collectively as $\phi \equiv \{\phi_1, \dots, \phi_\chi\}$. The number of fields per edge plays the role of bond dimension. We group the fields entering each vertex in two sets labeled as L and R . Generic Gaussian weights have the form

$$\phi_L \text{---} \text{---} \phi_R = \rho \exp \left(-\frac{1}{2} \phi_L^T A_L \phi_L - \frac{1}{2} \phi_R^T A_R \phi_R + \phi_L^T B \phi_R \right), \quad (4)$$

with $A_{L,R}$ and B as real matrices of dimension $2\chi \times 2\chi$ and ρ as a constant. We search for a decomposition of W inspired from the SVD. Namely, we want to factorize the dependence on L and R fields by introducing new variables, which according to the previous requirements should have the interpretation of fields,



$$\phi_L \text{---} \text{---} \phi_R = \phi_L \text{---} \text{---} \pi \text{---} \text{---} \phi_R \quad (5)$$

A way to proceed is working directly with the quadratic forms that appear in the exponent of the Gaussian weights. The L and R fields are connected by the matrix B , which, thus, hinders factorization. Since B is real, we have $B = UDV^T$ with U and V also real. We are assuming that D contains only strictly positive entries, and hence, it is of dimension $\tilde{\chi} = \text{rank}(B) \leq 2\chi$. Introducing $\tilde{\chi}$ new fields π , we can rewrite

$$W(\phi_L, \phi_R) = \rho G_L(\phi_L) \widehat{W}(\phi_L, \phi_R) G_R(\phi_R), \quad (6)$$

where we have used straightforward Gaussian integrations to define

$$\widehat{W} = \int d\pi e^{i\phi_L^T U \pi} S(\pi) e^{-i\pi^T V^T \phi_R} \quad (7)$$

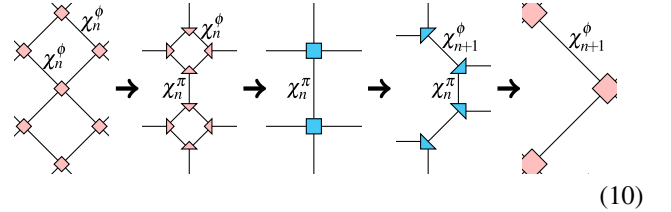
$$S = \frac{1}{\sqrt{(2\pi)^{\tilde{\chi}} \det D}} e^{-(1/2)\pi^T D^{-1} \pi}. \quad (8)$$

Relation (7) is a continuous SVD with the entries of the diagonal matrix S providing the singular values. π 's act as canonically conjugate variables of the original fields. However, the diagonal factors $G_{L,R}$ cause (6) to deviate from a SVD,

$$G_L = e^{-(1/2)\phi_L^T (A_L - UDU^T)\phi_L}, \quad G_R = e^{-(1/2)\phi_R^T (A_R - VDV^T)\phi_R}. \quad (9)$$

These matrices will prove crucial in the implementation of the TRG. They are the price to pay for the enormous simplification of working at the level of the exponent, dealing only with finite-dimensional matrices. We will refer to (6) as a Gaussian SVD (gSVD).

The Gaussian version of the TRG protocol we propose is an iterative application of the following transformations of a model defined on a lattice of N sites into a lattice of $N/2$ sites,



$$\text{---} \rightarrow \text{---} \rightarrow \text{---} \rightarrow \text{---} \quad (10)$$

namely: (i) gSVD of the weights of the ϕ fields, (ii) construction of the weights of the π fields, (iii) gSVD of the weights of the π fields, and (iv) construction of the weights of the ϕ fields. The ϕ and π fields turn out to have very different properties (see below). We will label the associated matrices with a subscript ϕ or π , corresponding to the tilted and directed lattices that are rotated by 45° every TRG transformation. A complete RG cycle returns to the same type of lattice, and thus, it is composed of two TRG steps.

We will use a subindex n to label the RG iteration as indicated in Eq. (10). The initial lattice has by assumption $\chi_1^\phi = 1$. B_1^ϕ has two equal singular values, implying $\chi_1^\pi = 2$. The bond dimension of the lattice emerging from the gSVD at any of the following steps is twice that of the fields running in the previous loop. Namely, $\chi_{n+1}^\phi = 2\chi_n^\phi$ in (10). The same holds for π fields as derived in detail in Appendix A. Hence, with no truncation $\chi_n^\phi = 2^{n-1}$ and $\chi_n^\pi = 2^n$, implying that the bond dimension doubles when transforming from ϕ to π fields, and remains constant in the next π to ϕ step.

The singular values added at each RG transformation are expected to encode correlations at larger coarse-grained scales. In the vacuum of the bosonic theory, correlations decay with distance. Hence, at some RG step, the newly added singular values should start being sufficiently small to set them to zero with a small error cost. This reduces the dimension of the ancillary field space and renders the calculation feasible. Since we are not dealing with an ordinary SVD, there is some degree of ambiguity involved in this implementation. We will

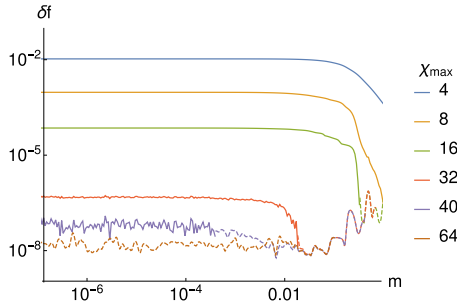


FIG. 1. Relative error in the free energy per site δf as a function of the mass m for a lattice with $L_1 = L_2 = 2^{30}$ and maximal bond dimensions χ_{\max} .

proceed as follows. The matrix B can be rewritten as

$$B = U_1 D_1 V_1^T + U_2 D_2 V_2^T, \quad (11)$$

where D_i are diagonal matrices with the highest ($i = 1$) and smallest ($i = 2$) eigenvalues of B respect to a chosen cutoff. Based on that, we can substitute

$$S(\pi) \rightarrow S_1(\pi_1)\delta(\pi_2). \quad (12)$$

The matrix S_1 is given by (8) with D replaced by D_1 . The δ function eliminates the dependence on the fields π_2 , reducing the bond dimension.

In terms of the original fields, the difference between the exact and the truncated weights comes from the limit $|\phi| \rightarrow \infty$. Therefore, in order to justify (12), it is necessary to have their large values suppressed. This is achieved by the factors $G_{L,R}$, which, in particular, contain the mass terms. The high accuracy of the numerical results presented below indicates that these matrices, indeed, play efficiently the role of field regulators.

We name this adapted TRG protocol gTRG. The integration leading to the new weights at each gTRG step are Gaussian and, thus, easy to perform. From now on, we use a scheme in which $U = V$, and hence, the relation $A_L = A_R$ satisfied by the initial weights will be preserved (see Appendix A). In this scheme, the same gSVD data characterize every lattice site.

IV. RESULTS

The partition function of a free boson can be computed analytically using momentum eigenmodes. For a lattice of size $L_1 \times L_2$ with periodic boundary conditions, it reads

$$Z_{L_1 L_2}^{\text{exact}} = \left(\frac{\pi}{2}\right)^{(L_1 L_2 / 2)} \prod_{n_1, n_2} \left(\sin^2 \frac{\pi n_1}{L_1} + \sin^2 \frac{\pi n_2}{L_2} + \frac{m^2}{4} \right)^{-(1/2)}, \quad (13)$$

where $n_i = 1, \dots, L_i$ ($i = 1, 2$). Comparison with the exact result allows us to test the performance of the gTRG method. In Fig. 1, we plot the relative error δf in the free energy per site $f = -\ln Z/L_1 L_2$ as a function of the mass for different maximal bond dimensions χ_{\max} . A large lattice with $L_1 = L_2 = 2^{30}$ has been chosen. With $\chi_{\max} = 32$, we obtain an error below 10^{-6} . The results for $\chi_{\max} > 32$ become increasingly noisy because we reach the accuracy limit, given by the precision for the inversion of matrices. The dashed lines

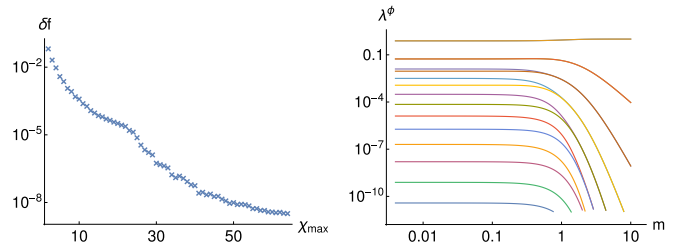


FIG. 2. Left: δf for $m = 1.2 \times 10^{-6}$ as a function of the bond dimension for $L_1 = L_2 = 2^{30}$. Right: Singular values of B_4^ϕ with no truncation. For large masses, they always join in equal value pairs. The two top curves correspond to doubly degenerate singular values.

in Fig. 1 are averaged results for the absolute value of δf , computed by applying a Gaussian filter of radius $\Delta \ln(m) = 0.14$. With $\chi_{\max} = 64$, the average precision is 10^{-8} , whereas, in the best cases, we have reached an error below 10^{-9} . Figure 2(left) shows the relative error in the free energy per site as a function of the bond dimension for $m = 1.2 \times 10^{-6}$, which, indeed, drops below 10^{-8} for large χ .

Truncation is first introduced in a step leading from a ϕ to a π lattice since it is then when the bond dimension increases. Figure 2(right) shows the singular values of B_4^ϕ . No truncation has been yet applied, and hence, $\chi_4^\phi = 8$. We observe that the singular values are very strongly decaying. This general property allows us to truncate them affecting, only mildly, the accuracy of the results. Notably it also holds in the limit of very small masses, explaining the smooth and efficient behavior of the gTRG in a regime which is problematic for the ordinary TRG.

Independently of the bond dimension, we have discarded singular values smaller than a threshold ϵ in order to minimize numerical errors. The value of ϵ depends on the numerical precision with which we are operating. In our case, we found it appropriate to set $\epsilon = 10^{-11}$.

Massless case

The accurate results of the gTRG for small masses allow us to address the massless case and, in particular, to compute the central charge. In the limits $m \ll 1$ and $L_1, L_2 \gg 1$ with L_2/L_1 constant, the exact partition function (13) can be approximated by (see Appendix D)

$$Z_{L_1 L_2}^{\text{exact}} \simeq \frac{e^{-f_\infty L_1 L_2}}{m(L_1 L_2)^{1/2}} Z_{\text{CFT}}(\tau), \quad (14)$$

where $f_\infty = \frac{2G}{\pi} - \frac{\ln 2\pi}{2}$ is the large lattice limit of the free energy per site with G as the Catalan constant. Z_{CFT} is the partition function of a massless boson in a torus with moduli parameter τ [41]. In our case, $\tau = iL_2/L_1$.

The CFT partition function is responsible for the leading finite-size corrections. Choosing $L_1 = L_2 \equiv L$, (14) yields

$$\frac{\pi}{6}c = L^2(f_\infty - f_L) + \ln(mL) + 2 \sum_{n=1}^{\infty} \ln(1 - e^{-2\pi n}), \quad (15)$$

where $c = 1$ is the theoretical value of the central charge [42,43]. Taking $L = 2^6$ and 2^7 and using (15) with f_L

computed numerically for $\chi_{\max} = 64$, we obtain, respectively,

$$c - 1 = O(10^{-5}), O(10^{-6}). \quad (16)$$

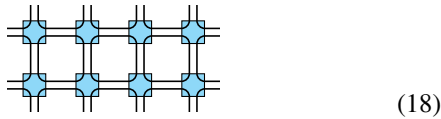
These values are derived averaging over $m \in [10^{-14}, 10^{-8}]$ in order to minimize the effect of the numerical noise on (15), which grows as the square of the lattice size. Noise wins over the leading finite-size effect for larger L , whereas for smaller lattices higher-order finite-size effects worsen the result. Equation (16) provides a check of the gTRG in the regime of intermediate size lattices, complementary to that explored in Fig. 1.

V. RG FLOW

The RG behavior of free field theories is extremely simple. When a mass parameter is present, it runs with the scale according to its bare dimension. Hence, a small mass will become of order one in lattice units after

$$n(m) \sim -\frac{\ln m}{\ln 2}, \quad (17)$$

RG iterations. For $n \gtrsim n(m)$, correlations should be mostly confined to occur inside a single lattice plaquette. Entanglement inside a plaquette is modeled by a CDL structure [31],



The TRG has the drawback of being unable to eliminate such ultralocal entanglement and reach a trivial IR fixed point. Instead, it promotes the inner correlations from half of the plaquettes to the next coarse-graining level, reproducing again a CDL structure [31]. The same should apply to the gTRG.

Due to the factorized nature of the CDL vertex, B is the direct sum of two equal matrices and, thus, its singular values come in pairs. In fact, the singular values of B^ϕ have always a strong tendency to arrange in pairs. Figure 2(right) shows that the six highest singular values have already paired up after three RG cycles. This is, however, not the case for B^π . For the first RG cycle, its two singular values can be derived explicitly,

$$\lambda_{1,1}^\pi = \frac{1}{m^2} \frac{8 + 4m^2 + m^4}{8 + 6m^2 + m^4}, \quad \lambda_{1,2}^\pi = \frac{1}{2 + m^2}. \quad (19)$$

For small masses, $\lambda_{1,1}^\pi \approx 1/m^2$ and $\lambda_{1,2}^\pi \approx 1/2$. We observe that, in successive RG cycles, the gap between the largest singular value and the rest slowly decreases until it closes. The singular values then pair up as required for CDL behavior and acquire fixed values. The smaller the mass, the larger the gap, and the more RG iterations are necessary. Figure 3 (left) shows the RG flow of the singular values for $m = 10^{-5}$ and $\chi_{\max} = 24$. Pairing is effective for $n \simeq 19$ in agreement with (17), which gives $n(10^{-5}) \simeq 16$ to 17.

The same behavior is seen in Fig. 3 (right). We have plotted the singular values of B_8^π obtained with $\chi_{\max} = 8$. The singular values pair up for masses larger than $m \approx 0.03$. Below, they rapidly unpair with the largest singular value strongly detaching from the rest. In rescaled lattice units,

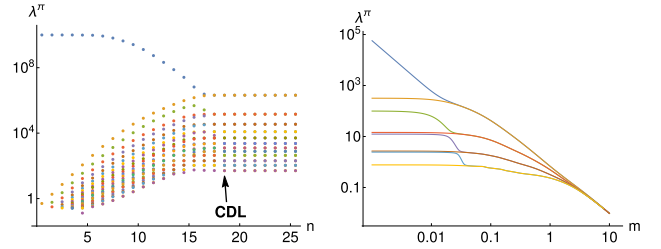


FIG. 3. Singular values of B_n^π . Left: RG flow for $m = 10^{-5}$ and $\chi_{\max} = 24$. Right: As a function of the mass for $n = 8$ and $\chi_{\max} = 8$.

the threshold mass is $0.03 \times 2^8 \approx 8$. Hence, a CDL structure does not emerge until scales larger than the correlation length $\xi = 1/m$ are reached.

Let us denote by \hat{B} the submatrix of B that connects fields on opposite links. Although the pairing of singular values is necessary for CDL, the vanishing of \hat{B} in two successive gTRG steps is a sufficient condition (see Appendix C). We define

$$P_{\text{CDL}} = \frac{1}{\chi} \frac{\|\hat{B}\|}{\lambda_1}, \quad (20)$$

where $\|\cdot\|$ is the Frobenius norm and λ_1 is the largest singular value of B . The RG evolution of this quantity is plotted in Fig. 4 (left) for the example of Fig. 3 (left). It abruptly decreases at the same scale at which the singular values pair up, confirming that the complete CDL structure is realized.

Figure 4 (right) shows the number of RG cycles necessary to attain a CDL IR fixed point using for criterium $P_{\text{CDL}} < 10^{-7}$. Similar results are obtained for large and small bond dimensions. In both cases, they are consistent with the scaling argument (17). An extrapolation to the massless limit implies $n \rightarrow \infty$ and, thus, an infinite correlation length. This suggests that the gTRG keeps some long-distance information for any bond dimensions. The reason behind it could be related to an important feature of the gTRG. It is constructed such that the lattice variables are always fields, which can take arbitrarily large values. As a consequence the diagonal matrix S in (7), whose components play the role of singular values for the gSVD, contains arbitrarily small entries even after truncation. On the contrary, the ordinary TRG discards the singular values smaller than a chosen cutoff.

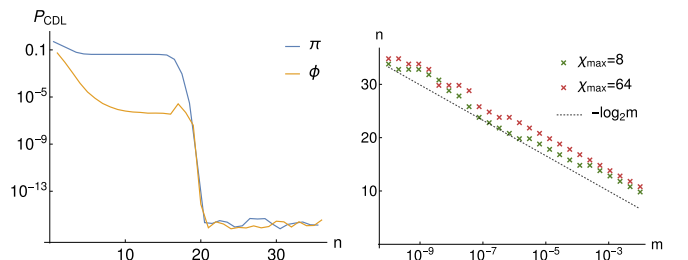


FIG. 4. Left: Indicator P_{CDL} for $m = 10^{-5}$ and $\chi_{\max} = 24$. The step at which it drops coincides with Fig. 3 (left). Right: RG cycles needed to reach a CDL structure. The theoretical argument (17) is shown in black.

VI. CONCLUSIONS

We have implemented the tensor renormalization-group method to compute the partition function of a free boson in two Euclidean dimensions. The guiding principle is to preserve the Gaussian character of the statistical weights. This led us to modify the singular value decomposition to handle continuous degrees of freedom taking unbounded values. We have obtained very accurate numerical results keeping a small number of fields in the RG iteration procedure. There is still some residual short-range entanglement that give rise to CDL tensors. We expect that a version of the TNR along the lines of Refs. [32,33] would eliminate it completely reducing the computational cost to achieve the same accuracy as it occurs for spin models.

We expect that our results serve as a starting point for a perturbative treatment of interacting models. In this construction, the gSVD should play the role that free theory propagators have in the construction of interacting field theories. This will allow us to get new insights on the interplay between entanglement and interactions. The final goal is to improve the performance of the entanglement-based RG method in quantum-field theory.

ACKNOWLEDGMENTS

We would like to thank M. C. Bañuls, J. I. Cirac, G. Evenbly, M. García-Pérez, E. Kim, J. I. Latorre, C. Pena, S. Ryu, L. Tagliacozzo, and G. Vidal for conversations. We acknowledge financial support from Grants No. FPA2015-65480-P, No. FIS2015-69167-C2-1-P, No. PGC2018-095862-B-C21, No. QUITEMAD + S2013/ICE-2801, and No. SEV-2016-0597 of the ‘‘Centro de Excelencia Severo Ochoa’’ Programme.

APPENDIX A: gTRG ALGORITHM

In order to apply the gTRG algorithm, we first write the bosonic partition function as a contraction of a square tensor network in which each tensor is given by Eq. (2),

$$W_1^\phi(\phi) = \rho_1 e^{-(1/2)\phi^T M_1^\phi \phi}, \quad \rho_1 = 1, \quad M_1 = \frac{m^2}{2} \mathbb{1}_4 + K, \quad (A1)$$

$$K = \begin{pmatrix} 2 & -1 & -1 & 0 \\ -1 & 2 & 0 & -1 \\ -1 & 0 & 2 & -1 \\ 0 & -1 & -1 & 2 \end{pmatrix},$$

with $\phi = (\phi_1, \phi_2, \phi_4, \phi_3)$ as indicated in (3). Similarly, at each step, we will have square lattices of tensors W_n^φ , where n indicates the RG cycle and φ represents the ϕ or π fields. The goal of the gTRG algorithm is to compute from W_n^φ its coarse-grained version $W_{\tilde{n}}^{\tilde{\varphi}}$. If $\varphi = \phi$, then $\tilde{\varphi} = \pi$ and $\tilde{n} = n$, whereas if $\varphi = \pi$, then $\tilde{\varphi} = \phi$ and $\tilde{n} = n + 1$. Namely, $W_n^\phi \rightarrow W_n^\pi$ and $W_n^\pi \rightarrow W_{n+1}^\phi$.

From now on, when no confusion is possible, we just write $W_n^\varphi = W$ and $W_{\tilde{n}}^{\tilde{\varphi}} = \tilde{W}$. Following the TRG, we use the gSVD to split $W(\varphi) = \exp(-\frac{1}{2}\varphi^T M \varphi)$ in left and right tensors as shown in Eq. (4). Accordingly we separate the fields φ in their left and right components $\varphi_L = (\varphi_1, \varphi_2)$ and $\varphi_R = (\varphi_3, \varphi_4)$, where φ_i 's collectively denote all fields that live in the corresponding lattice link. M is then decomposed

in four blocks,

$$M = \begin{pmatrix} A & -B \\ -B & A \end{pmatrix}. \quad (A2)$$

As we will show, those blocks have further structures, and it is possible to decompose them as

$$A - B = \frac{1}{2} \begin{pmatrix} s & 0 \\ 0 & s \end{pmatrix} + \begin{pmatrix} a & -a \\ -a & a \end{pmatrix},$$

$$B = \frac{1}{2} \begin{pmatrix} b_+ + b_- & b_+ - b_- \\ b_+ - b_- & b_+ + b_- \end{pmatrix}, \quad (A3)$$

where a , b_+ , and b_- are $\chi \times \chi$ symmetric and positive semidefinite matrices and s is a $\chi \times \chi$ diagonal matrix with non-negative entries. The matrices s , a , and b_\pm act on the fields φ_i of each separated lattice link. This structure is verified by the initial weights where those small blocks are just numbers,

$$s_1 = m^2, \quad a_1^\phi = b_{+,1}^\phi = b_{-,1}^\phi = 1. \quad (A4)$$

The proof proceeds by induction. We assume that the previous structure is realized by W . Now, we perform the gSVD of W using the SVD of B as explained in the body of the article. Since we have assumed that b_\pm 's are positive definite, so is B , and its SVD reduces to a diagonalization. The diagonalization of $B = UDU^T$ can be computed from the diagonalization of its blocks $b_\pm = u_\pm d_\pm u_\pm^T$. The isometries u_\pm span the space of nonzero eigenvalues, and d_\pm is the diagonal matrix with the nonzero eigenvalues of b_\pm . The $\tilde{\chi} \times \tilde{\chi}$ diagonal matrix D and $2\chi \times \tilde{\chi}$ isometry U are

$$D = \begin{pmatrix} d_+ & 0 \\ 0 & d_- \end{pmatrix}, \quad U = \frac{1}{\sqrt{2}} \begin{pmatrix} u_+ & u_- \\ u_+ & -u_- \end{pmatrix}. \quad (A5)$$

At this point, if the number of new fields $\tilde{\chi}$ is too big or some of the eigenvalues in D are too small, we can implement the truncation as explained in the main text.

In the original TRG algorithm, each tensor of the lattice is split in two $W = V\tilde{V}^\dagger$. The gTRG algorithm proceeds in the same way. Due to the assumed structure of W we have $V = \tilde{V}$ so that

$$W(\varphi_L, \varphi_R) = \int d\tilde{\varphi} V(\varphi_L, \tilde{\varphi}) V^\dagger(\tilde{\varphi}, \varphi_R). \quad (A6)$$

This relation can be written pictorially as

$$\begin{array}{c} \varphi_1 \quad \varphi_3 \\ \diagdown \quad \diagup \\ \text{---} W \text{---} \\ \diagup \quad \diagdown \\ \varphi_2 \quad \varphi_4 \end{array} = \begin{array}{c} \varphi_1 \quad \varphi_3 \\ \diagdown \quad \diagup \\ \text{---} V \text{---} \tilde{\varphi} \text{---} V^\dagger \text{---} \\ \diagup \quad \diagdown \\ \varphi_2 \quad \varphi_4 \end{array}, \quad (A7)$$

where from Eqs. (6)–(9),

$$V(\varphi_L, \tilde{\varphi}) = \sqrt{\rho} G(\varphi_L) e^{i\varphi_L^T U \tilde{\varphi}} S^{1/2}(\tilde{\varphi}). \quad (A8)$$

To obtain the new tensor \tilde{W} , we have to contract a loop of four tensors V . Depending on how we label the two halves of each tensor W , left and right, we can have different resulting tensors \tilde{W} that are equivalent under a suitable change of fields $\varphi \rightarrow -\varphi$. We are going to fix this freedom in such a way that all \tilde{W} 's are equal up to 90° rotation since, at the next step, they will be split along a different axis and have the structures

showed at (A2) and (A3). Our choice can be depicted as

$$\begin{array}{c} \tilde{\varphi}_3 \\ \nearrow \quad \nwarrow \\ \varphi_1 \quad \varphi_4 \\ \searrow \quad \swarrow \\ \varphi_2 \quad \tilde{\varphi}_3 \\ \downarrow \\ \tilde{\varphi}_2 \end{array} = \begin{array}{c} \tilde{\varphi}_3 \\ \square \\ \tilde{\varphi}_2 \end{array} \begin{array}{c} \tilde{\varphi}_1 \\ \leftarrow \\ \tilde{\varphi}_4 \end{array} \quad (\text{A9})$$

The resulting lattice of tensors preserves the translational and rotational symmetries of the original lattice but only at the level of plaquettes as can be seen in the following figure:

$$\begin{array}{cccc} \square & \square & \square & \square \\ \square & \square & \square & \square \end{array} \quad (\text{A10})$$

The new tensor $\tilde{W}(\tilde{\varphi})$ is given by

$$\begin{aligned} \tilde{W}(\tilde{\varphi}) &= \int \prod_{i=1}^4 d\varphi_i V(\varphi_1, \varphi_2; \tilde{\varphi}_1) V^\dagger(\tilde{\varphi}_2; \varphi_2, \varphi_3) \\ &\quad \times V(\varphi_3, \varphi_4; \tilde{\varphi}_4) V^\dagger(\tilde{\varphi}_3; \varphi_4, \varphi_1) \\ &= \tilde{\rho} e^{-(1/2)\tilde{\varphi}^T \tilde{M} \tilde{\varphi}}. \end{aligned} \quad (\text{A11})$$

with

$$\tilde{M} = \frac{1}{2} \mathbf{1}_4 \otimes D^{-1} + C^T Q^{-1} C, \quad \tilde{\rho} = \rho^2 \frac{(2\pi)^{2\chi - \tilde{\chi}}}{\det(D) \det(Q)^{1/2}}. \quad (\text{A12})$$

The matrix Q collects terms quadratic in φ in the exponent of the integrand and C collects the cross terms in φ and $\tilde{\varphi}$, whereas ρ is the corresponding factor of W . It is convenient to decompose C in two blocks such that $\varphi^T C \tilde{\varphi} = \varphi^T C_L \tilde{\varphi}_L + \varphi^T C_R \tilde{\varphi}_R$. We have

$$\begin{aligned} Q &= \mathbf{1}_4 \otimes s + K \otimes a, \quad C_L = \begin{pmatrix} U & 0 \\ 0 & 0 \end{pmatrix} - S \begin{pmatrix} 0 & 0 \\ 0 & U' \end{pmatrix}, \\ C_R &= \begin{pmatrix} 0 & 0 \\ 0 & U \end{pmatrix} - S \begin{pmatrix} U' & 0 \\ 0 & 0 \end{pmatrix}, \end{aligned} \quad (\text{A13})$$

where U' is defined as U in (A5) but substituting u_- by $-u_-$ and the $4\chi \times 4\chi$ matrix S shifts φ_i to φ_{i-1} . Straightforward manipulations show that \tilde{W} has the structure described in (A2) and (A3) with

$$\begin{aligned} \tilde{s} &= D^{-1}, \quad \tilde{a} = U^T \begin{pmatrix} 0 & 0 \\ 0 & q_1 \end{pmatrix} U, \quad \tilde{b}_+ = U^T \begin{pmatrix} q_1 & 0 \\ 0 & 0 \end{pmatrix} U, \\ \tilde{b}_- &= \frac{1}{2} U^T \begin{pmatrix} q_0 + q_2 & q_0 - q_2 \\ q_0 - q_2 & q_0 + q_2 - 2q_1 \end{pmatrix} U, \end{aligned} \quad (\text{A14})$$

where $q_j = (s + 2ja)^{-1}$. The matrix \tilde{s} is diagonal with non-negative entries. The matrices \tilde{a} , \tilde{b}_+ , and \tilde{b}_- are symmetric by construction. They are also positive semidefinite. This is evident for \tilde{a} and \tilde{b}_+ since their eigenvalues are those of q_1 , which is positive semidefinite because so are s and a by assumption. After some simple algebra, \tilde{b}_- is also shown to be positive semidefinite.

When the eigenvalues of b_\pm are all nonvanishing, $\tilde{\chi} = \text{rank}(B) = 2\chi$ and U is an orthogonal matrix. In this case, expressions (A15) make clear that the matrices \tilde{a} and \tilde{b}_+ have half of their eigenvalues equal to zero. It can be seen that the

same result holds for \tilde{b}_- . As a consequence, when we perform a new gTRG iteration, the bond dimension does not increase

$$\chi^{\text{new}} = \text{rank}(\tilde{B}) = \text{rank}(\tilde{b}_+) + \text{rank}(\tilde{b}_-) = \tilde{\chi}. \quad (\text{A15})$$

Moreover \tilde{U} is a $2\tilde{\chi} \times \tilde{\chi}$ isometry, and (A15) does not restrict the number of positive eigenvalues of the matrices a^{new} , b_\pm^{new} . In the generic case, all of them will be nonvanishing. In the initial lattice (A4), $b_{\pm,1}$'s have trivially maximal rank. Therefore, without truncation, $\chi_n^\pi = 2\chi_n^\phi$ and $\chi_{n+1}^\phi = \chi_n^\pi$.

Computation of the partition function

In this article, we compute the partition function of square lattices with L^2 sites and periodic boundary conditions with $L = 2^S$. After each gTRG step, the number of sites is reduced by 1/2. Therefore, after $S - 1$ RG steps, our lattice only has four sites, and there are only two tensors left. Then, performing another gTRG transformation, the lattice becomes the tensor trace of just one tensor W_S^π ,

$$Z = \text{tTr} W_S^\pi = \int d\pi_1 d\pi_2 W_S(\pi_1, \pi_2, \pi_2, \pi_1) = \text{Tr} \left(\square W_S^\pi \right). \quad (\text{A16})$$

It is important to take into account that the definition of the tensor W_S^π in the last step is special since we are not free to arrange the loop of tensors as in (A9). Instead, we are forced to use a disposition in which V_S^ϕ and $(V_S^\phi)^\dagger$ are placed at opposite sides as in the following figure:

$$\begin{array}{c} \square \\ \square \\ \square \\ \square \end{array} = \begin{array}{c} \square \\ \square \\ \square \\ \square \end{array} \quad (\text{A17})$$

APPENDIX B: DETAILS OF THE TRUNCATION

In order to minimize the numerical error, the gTRG discards singular values of B below a given threshold ϵ . Without truncation, the singular values of B_n^ϕ follow an approximately exponential distribution with smaller values added at each step, see Fig. 2(left). If we allow χ_{max} large enough, at some point, some of them will be smaller than ϵ . Using the value of $\epsilon = 10^{-11}$, this happens when $\chi_{\text{max}} > 22$ for $m < 0.1$ and at smaller χ_{max} for bigger masses. Truncations which involve ϵ have relevant differences with those in which ϵ plays no role. In the latter case, truncation only starts when the maximal bond dimension χ_{max} is reached. Before that, the bond dimensions double in the gTRG steps that lead from ϕ to π fields and remain constant when transforming from π to ϕ fields. Therefore,

$$\chi_{n-1}^\pi = \chi_n^\phi = \frac{1}{2} \chi_n^\pi. \quad (\text{B1})$$

A typical sequence is provided by $m = 10^{-6}$ and $\chi_{\text{max}} = 20$,

$$\begin{aligned} \{ \chi_1^\phi, \chi_1^\pi, \chi_2^\phi, \chi_2^\pi, \dots \} \\ = \{ 1, 2, 2, 4, 4, 8, 8, 16, 16, 20, 20, 20, 20, \dots \}. \end{aligned} \quad (\text{B2})$$

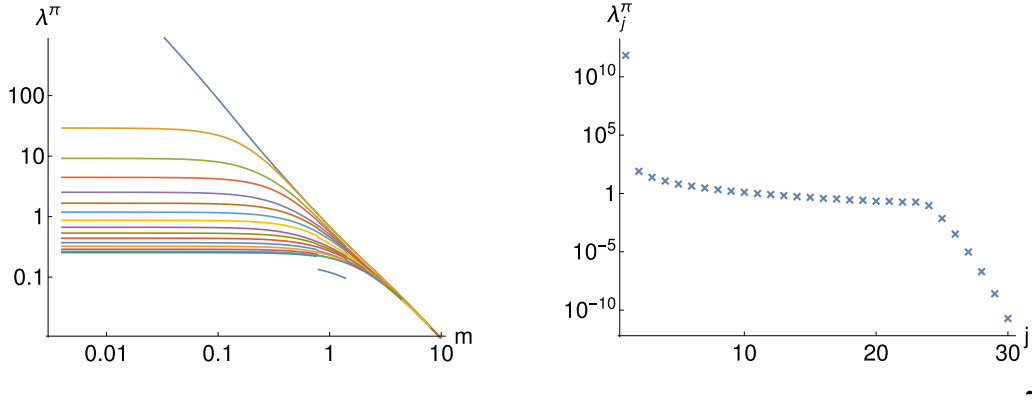


FIG. 5. Left: Singular values of B_4^π without truncation. For small masses, the largest singular value is approximately m^{-2} . For large masses, they all converge to m^{-2} . Right: Singular values of B_5^π for $m = 10^{-6}$.

On the contrary, if $\chi_{\max} = 64$, we have

$$\begin{aligned} & \{\chi_1^\phi, \chi_1^\pi, \chi_2^\phi, \chi_2^\pi, \dots\} \\ & = \{1, 2, 2, 4, 4, 8, 8, 16, 16, 22, 30, 35, 41, 46, \\ & \quad 54, 60, 64, 64, 64, 64, \dots\}. \end{aligned} \quad (\text{B3})$$

In this case, truncation is first triggered by ϵ , and several iterations are needed to achieve the maximal bond dimension.

Before truncation, the matrices B_n^π have quite different properties from B_n^ϕ : (i) half of their singular values are zero, and (ii) those nonvanishing stay above $O(1)$ values. The singular values of B_4^π are shown for the illustration in Fig. 5(left). Once, ϵ triggers truncation $\chi_n^\pi < 2\chi_n^\phi$ as seen in (B3). Moreover, the two previous properties of B_n^π are not satisfied anymore. More than half of its singular values are now positive. The largest χ_n^π 's of them behave as before. The new ones, instead, decay in an approximately exponential way, similar to those of the ϕ lattices. In Fig. 5(right), we show the singular values of the matrix B_5^π associated with (B3). We observe that the first $\chi_5^\pi = 22$ singular values stay above $O(1)$, whereas the next ones strongly decay. A total number of $\chi_6^\phi = 30$ survive the ϵ cutoff. Hence, after truncation is triggered $\chi_n^\phi > \chi_{n-1}^\pi$.

The resulting stepwise pattern of reaching the maximal bond dimension has important consequences in the performance of the gTRG. In Fig. 2(left), we have plotted the relative error in the free energy as a function of the maximal bond dimension for $m = 1.2 \times 10^{-6}$. This curve has two differentiated segments. The first one falls as χ^{-a} with $a \sim 3.44$. This is the typical TRG behavior in which improving the precision is increasingly expensive [28,32]. The parameter ϵ starts playing a role at $\chi_{\max} = 22$. At this point, the curve enters its second segment where we observe that the precision improves at a lower computational cost. Interestingly, this turns out to rely on the possibility of having $\chi_n^\phi > \chi_{n-1}^\pi$. Indeed, we have checked that restricting the bond dimensions to only increase in the ϕ to π transformations clearly worsens the results.

APPENDIX C: CDL STRUCTURE

In this Appendix, we explain the details of the CDL structure that appears in the gTRG algorithm. The internal structure

of the CDL tensors is given by

$$e^{-(1/2)\varphi^T M_{\text{CDL}} \varphi} \propto \varphi_1 \begin{array}{c} \varphi_3 \\ \text{---} \\ \text{---} \\ \text{---} \\ \varphi_2 \end{array} \varphi_4.$$

where the internal lines represent cross terms between the corresponding fields in the exponent. The matrix M_{CDL} factorizes, thus, in the tensor product of four equal blocks,

$$\begin{aligned} M_{\text{CDL}} &= \mathbb{1}_4 \otimes m_{\text{CDL}}, \\ m_{\text{CDL}} &= \mathbb{1}_2 \otimes h + \begin{pmatrix} 1 & -1 \\ -1 & 1 \end{pmatrix} \otimes k, \quad m_{\text{CDL}} \sim \begin{array}{c} \text{---} \\ \text{---} \\ \text{---} \\ \text{---} \end{array} \end{aligned} \quad (\text{C1})$$

where h and k are $\chi/2 \times \chi/2$ symmetric positive definite real matrices.

In terms of the definitions introduced in Appendix A, CDL requires: (i) $b_+ = b_-$, (ii) half of the eigenvalues of a and b_+ are zero, (iii) the subspaces spanned by the eigenvectors of a and b_+ with nonzero eigenvalues are orthogonal, (iv) the mass matrix s does not connect these subspaces. We will now show that, if the submatrices b_\pm coincide in two consecutive gTRG steps, or equivalently, a RG cycle, then the full CDL structure is realized. The indicator P_{CDL} defined in (20), where $\hat{B} = (b_+ - b_-)/2$, measures the deviation from this condition. Following the notation of Appendix A, we label two consecutive gTRG steps with indices n and \tilde{n} and their associated fields by φ and $\tilde{\varphi}$. We assume $b_+ = b_-$ and $\tilde{b}_+ = \tilde{b}_-$. The matrix $b \equiv b_+ = b_-$ decomposes as udu^T where the $\tilde{\chi}/2 \times \tilde{\chi}/2$ diagonal matrix d collects its positive eigenvalues and u is a $\chi \times \tilde{\chi}/2$ isometry. Using (A15) and further applying the following change of basis to the fields in each lattice link,

$$\mathbb{1}_{\tilde{\chi}/2} \otimes \frac{1}{\sqrt{2}} \begin{pmatrix} 1 & 1 \\ 1 & -1 \end{pmatrix}, \quad (\text{C2})$$

we obtain

$$\begin{aligned} \tilde{s} &= \begin{pmatrix} d^{-1} & 0 \\ 0 & d^{-1} \end{pmatrix}, \quad \tilde{a} = \begin{pmatrix} 0 & 0 \\ 0 & u^T s^{-1} u \end{pmatrix}, \\ \tilde{b} \equiv \tilde{b}_+ = \tilde{b}_- &= \begin{pmatrix} u^T s^{-1} u & 0 \\ 0 & 0 \end{pmatrix}. \end{aligned} \quad (\text{C3})$$

These matrices clearly satisfy all the requirements for CDL and lead to (C1) with $h = d^{-1}$ and $k = u^T s^{-1} u$.

The CDL structure is a fixed point of the gTRG algorithm. Let us perform a gTRG iteration taking as a starting point (C3). The nonzero block of the matrices a and b has maximal rank, and thus, the new bond dimension is again $\chi_{n+1} = \tilde{\chi}$. This implies that $\tilde{b} = \tilde{u} \tilde{d} \tilde{u}^T$, where $\tilde{u}^T = (v^T \ 0)$ and v is the orthogonal matrix that diagonalizes $u^T s^{-1} u$. The building blocks of the new tensors $\tilde{q}_j = (\tilde{s} + 2j\tilde{a})^{-1}$ defined in (A15), satisfy

$$\tilde{u}^T \tilde{q}_j \tilde{u} = v^T d v. \quad (\text{C4})$$

Therefore $(b_+)_{n+1} = (b_-)_{n+1}$, and the complete CDL structure is realized with $h = \tilde{d}^{-1}$ and $k = v^T d v$. A new gTRG iteration leads to $h = d^{-1}$ and $k = v \tilde{d} v^T$, showing that a RG cycle leaves invariant the exponent of the Gaussian weights. Interestingly, a gTRG step exchanges the roles of h and k .

APPENDIX D: EXACT RESULTS AND RELATION WITH CONFORMAL FIELD THEORY

Let us consider a lattice $L_1 \times L_2$ and real scalar fields ϕ_{ij} , $i = 1, \dots, L_1$, $j = 1, \dots, L_2$. The partition function is given by

$$Z = \int \prod_{ij} d\phi_{ij} e^{-S[\phi]}, \quad (\text{D1})$$

with

$$S = \frac{1}{2} \sum_{i=1}^{L_1} \sum_{j=1}^{L_2} [(\phi_{ij} - \phi_{i+1j})^2 + (\phi_{ij} - \phi_{ij+1})^2 + m^2 \phi_{ij}^2]. \quad (\text{D2})$$

Let us make the Fourier transform,

$$\phi_{j_1 j_2} = \frac{1}{\sqrt{L_1 L_2}} \sum_{k_1, k_2} e^{i(k_1 j_1 + k_2 j_2)} \hat{\phi}_{k_1 k_2}, \quad (\text{D3})$$

where the periodic boundary conditions imply

$$k_i = \frac{2\pi n_i}{L_i} (n_i = 1, \dots, L_i), \quad i = 1, 2, \quad (\text{D4})$$

and the reality condition reads

$$\hat{\phi}_{k_1 k_2}^* = \hat{\phi}_{-k_1 -k_2}. \quad (\text{D5})$$

In momentum space, the action becomes

$$S = \frac{1}{2} \sum_{k_1, k_2} \left(4 \sin^2 \frac{k_1}{2} + 4 \sin^2 \frac{k_2}{2} + m^2 \right) \hat{\phi}_{k_1 k_2} \hat{\phi}_{k_1 k_2}^*. \quad (\text{D6})$$

Performing the Gaussian integration yields

$$Z(L_1, L_2) = (2\pi)^{L_1 L_2 / 2} \times \prod_{n_1, n_2} \left(4 \sin^2 \frac{\pi n_1}{L_1} + 4 \sin^2 \frac{\pi n_2}{L_2} + m^2 \right)^{-1/2}. \quad (\text{D7})$$

Relation with CFT

In the limit $m \rightarrow 0$, we can approximate Eq. (D7) by

$$Z(L_1, L_2) \simeq \frac{2}{m} \left(\frac{\pi}{2} \right)^{L_1 L_2 / 2} \times \prod_{(n_1, n_2) \neq (L_1, L_2)} \left(\sin^2 \frac{\pi n_1}{L_1} + \sin^2 \frac{\pi n_2}{L_2} \right)^{-1/2}. \quad (\text{D8})$$

We will compute this product in the limit $L_1, L_2 \gg 1$, keeping the ratio L_2/L_1 constant. For this purpose, we will employ the following formula:

$$\prod_{n=1}^L \left(x^2 + \sin^2 \frac{\pi n}{L} \right) = (2^{1-L} \sinh(L \operatorname{arcsinh}(x)))^2, \quad (\text{D9})$$

that using

$$\operatorname{arcsinh}(x) = \ln(x + \sqrt{1+x^2}) \quad (\text{D10})$$

becomes

$$\prod_{n=1}^L \left(x^2 + \sin^2 \frac{\pi n}{L} \right) = 2^{-2L} [(x + \sqrt{1+x^2})^L - (x + \sqrt{1+x^2})^{-L}]^2. \quad (\text{D11})$$

Let us write Eq. (D8) as

$$Z(L_1, L_2) \simeq \frac{2}{m} \left(\frac{\pi}{2} \right)^{L_1 L_2 / 2} \prod_{(n_1, n_2) \neq (L_1, L_2)} a(n_1, n_2), \quad (\text{D12})$$

where

$$a(n_1, n_2) = \left(\sin^2 \frac{\pi n_1}{L_1} + \sin^2 \frac{\pi n_2}{L_2} \right)^{-1/2}. \quad (\text{D13})$$

We can split the product in (D12) as

$$A \equiv \prod_{(n_1, n_2) \neq (L_1, L_2)} a(n_1, n_2) = \prod_{n_2=1}^{L_2-1} a(L_1, n_2) \prod_{n_1=1}^{L_1-1} \prod_{n_2=1}^{L_2} a(n_1, n_2). \quad (\text{D14})$$

The first factor is given by

$$\prod_{n_2=1}^{L_2-1} a(L_1, n_2) = \prod_{n_2=1}^{L_2-1} \left(\sin \frac{\pi n_2}{L_2} \right)^{-1} = (2^{1-L_2} L_2)^{-1}, \quad (\text{D15})$$

whereas the second factor can be obtained using (D11),

$$\begin{aligned} & \prod_{n_1=1}^{L_1-1} \prod_{n_2=1}^{L_2} a(n_1, n_2) \\ &= \prod_{n_1=1}^{L_1-1} \prod_{n_2=1}^{L_2} \left(\sin^2 \frac{\pi n_1}{L_1} + \sin^2 \frac{\pi n_2}{L_2} \right)^{-1/2} \\ &= 2^{L_2(L_1-1)} \prod_{n_1=1}^{L_1-1} [(x_{n_1} + \sqrt{1+x_{n_1}^2})^{L_2} - (x_{n_1} + \sqrt{1+x_{n_1}^2})^{-L_2}]^{-1} \end{aligned}$$

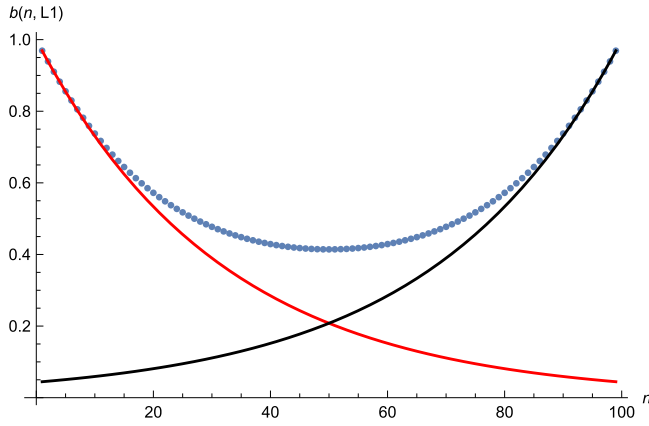


FIG. 6. Plot of the function $b(n, L_1)$ for $n = 1, \dots, L_1 - 1$ and $L_1 = 100$. The red curve is $e^{-\pi n_1/L_1}$, and the blue curve is $e^{-\pi(L_1-n_1)/L_1}$.

$$\begin{aligned}
 &= 2^{L_2(L_1-1)} \prod_{n_1=1}^{L_1-1} (x_{n_1} + \sqrt{1+x_{n_1}^2})^{-L_2} \\
 &\quad \times \prod_{n_1=1}^{L_1-1} [1 - (x_{n_1} + \sqrt{1+x_{n_1}^2})^{-2L_2}]^{-1}, \quad (\text{D16})
 \end{aligned}$$

where

$$x_{n_1} = \sin \frac{\pi n_1}{L_1}. \quad (\text{D17})$$

Combining Eqs. (D12), (D15), and (D16) yields

$$\begin{aligned}
 Z(L_1, L_2) &\simeq \frac{(2\pi)^{(1/2)L_1 L_2}}{m L_2} \prod_{n_1=1}^{L_1-1} (x_{n_1} + \sqrt{1+x_{n_1}^2})^{-L_2} \\
 &\quad \times \prod_{n_1=1}^{L_1-1} [1 - (x_{n_1} + \sqrt{1+x_{n_1}^2})^{-2L_2}]^{-1}. \quad (\text{D18})
 \end{aligned}$$

Let us define

$$\begin{aligned}
 b(n_1, L_1) &= (x_{n_1} + \sqrt{1+x_{n_1}^2})^{-1} \\
 &= -\sin \frac{\pi n_1}{L_1} + \sqrt{1 + \sin^2 \frac{\pi n_1}{L_1}}. \quad (\text{D19})
 \end{aligned}$$

Figure 6 shows that, for $L_1 \gg 1$, the values of this function near 1 can be approximated by

$$b(n_1, L_1) \simeq \begin{cases} e^{-\pi n_1/L_1}, & n_1 \ll L_1, \\ e^{-\pi(L_1-n_1)/L_1}, & n_1 \simeq L_1. \end{cases} \quad (\text{D20})$$

These analytic expressions can be derived from Eq. (D19). Hence, in the limit $L_1, L_2 \gg 1$ with L_2/L_1 constant, we find

$$\begin{aligned}
 &\prod_{n_1=1}^{L_1-1} [1 - (x_{n_1} + \sqrt{1+x_{n_1}^2})^{-2L_2}]^{-1} \\
 &\simeq \prod_{n_1=1}^{L_1-1} (1 - e^{-2\pi L_2 n_1/L_1})^{-2} \simeq \prod_{n=1}^{\infty} (1 - q^n)^{-2}, \quad (\text{D21})
 \end{aligned}$$

where

$$q = e^{-2\pi L_2/L_1}. \quad (\text{D22})$$

The exponent 2 in Eq. (D21) comes from the terms around $n_1 \simeq L_1$ that contribute with the same amount as those near $n_1 \ll L_1$.

Let us now evaluate the first product in Eq. (D18),

$$\prod_{n=1}^{L_1-1} (x_n + \sqrt{1+x_n^2})^{-L_2} = \exp\left(-L_2 \sum_{n=1}^{L_1-1} f(n)\right), \quad (\text{D23})$$

where

$$f(n) = \ln(x_n + \sqrt{1+x_n^2}) = \ln\left(\sin \frac{\pi n}{L_1} + \sqrt{1 + \sin^2 \frac{\pi n}{L_1}}\right). \quad (\text{D24})$$

To approximate the sum (D23), we use the Euler-MacLaurin formula,

$$\begin{aligned}
 \sum_{n=1}^{L_1-1} f(n) &= \int_0^{L_1} dn f(n) - \frac{f(0) + f(L_1)}{2} \\
 &\quad + \frac{1}{12}[f'(L_1) - f'(0)] + \dots, \quad (\text{D25})
 \end{aligned}$$

and compute the various terms,

$$\begin{aligned}
 \int_0^{L_1} dn f(n) &= L_1 \int_0^1 dx \ln[\sin(\pi x) + \sqrt{1 + \sin^2(\pi x)}] \\
 &= \frac{2G}{\pi} L_1, \quad (\text{D26})
 \end{aligned}$$

where G is the Catalan constant. The rest of the quantities are given in the limit $L_1 \gg 1$ by

$$\begin{aligned}
 f(0) &= f(L_1) = 0, \\
 f'(0) &= -f'(L_1) = \frac{\pi}{L_1} + O(L_1^{-3}). \quad (\text{D27})
 \end{aligned}$$

Therefore,

$$\sum_{n=1}^{L_1-1} f(n) \simeq \frac{2G}{\pi} L_1 - \frac{\pi}{6L_1}, \quad (\text{D28})$$

which plugged into Eq. (D23) yields

$$\begin{aligned}
 \prod_{n=1}^{L_1-1} (x_n + \sqrt{1+x_n^2})^{-L_2} &= \exp\left[-\frac{2G}{\pi} L_1 L_2 + \frac{\pi L_2}{6L_1}\right] \\
 &= \exp\left[-\frac{2G}{\pi} L_1 L_2\right] q^{-(1/12)}. \quad (\text{D29})
 \end{aligned}$$

Collecting terms, Eq. (D18) becomes

$$\begin{aligned}
 Z(L_1, L_2) &\simeq \frac{(2\pi)^{(1/2)L_1 L_2}}{m L_2} \exp\left[-\frac{2G}{\pi} L_1 L_2\right] \\
 &\quad \times q^{-(1/12)} \prod_{n=1}^{\infty} (1 - q^n)^{-2}, \quad (\text{D30})
 \end{aligned}$$

that can be written as

$$Z(L_1, L_2) \simeq \frac{e^{-L_1 L_2 f_\infty}}{m \sqrt{L_1 L_2}} Z_{\text{CFT}}(\tau), \quad (\text{D31})$$

where f_∞ is the free energy per site,

$$f_\infty = \frac{2G}{\pi} - \frac{\ln(2\pi)}{2}. \quad (\text{D32})$$

$Z_{\text{CFT}}(\tau)$ is the partition function of a massless boson on a torus with moduli parameter τ [41],

$$Z_{\text{CFT}}(\tau) = \frac{1}{(\text{Im } \tau)^{1/2} |\eta(q)|^2}, \quad q = e^{2\pi i \tau}, \quad \tau = i \frac{L_2}{L_1}, \quad (\text{D33})$$

and

$$\eta(\tau) = q^{1/24} \prod_{n=1}^{\infty} (1 - q^n) \quad (\text{D34})$$

is the Dedekind η function. Equation (D7) is symmetric under the exchange $L_1 \leftrightarrow L_2$, a condition that is guaranteed in (D33) by the modular invariance of Z_{CFT} ,

$$Z_{\text{CFT}}(\tau) = Z_{\text{CFT}}(-1/\tau). \quad (\text{D35})$$

-
- [1] F. Verstraete, J. I. Cirac, and V. Murg, Matrix product states, projected entangled pair states, and variational renormalization group methods for quantum spin systems, *Adv. Phys.* **57**, 143 (2008)
- [2] R. Orús, A practical introduction to tensor networks: Matrix product states and projected entangled pair states, *Ann. Phys. (NY)* **349**, 117 (2014).
- [3] I. Affleck, T. Kennedy, E. H. Lieb, and H. Tasaki, Valence bond ground states in isotropic quantum antiferromagnets, *Commun. Math. Phys.* **115**, 477 (1988).
- [4] M. Fannes, B. Nachtergaele, and R. F. Werner, Finitely correlated states on quantum spin chains, *Commun. Math. Phys.* **144**, 443 (1992).
- [5] A. Klümper, A. Schadschneider, and J. Zittartz, Matrix-product-groundstates for one-dimensional spin-1 quantum antiferromagnets, *Europhys. Lett.* **24**, 293 (1993).
- [6] S. Östlund and S. Rommer, Thermodynamic Limit of Density Matrix Renormalization, *Phys. Rev. Lett.* **75**, 3537 (1995).
- [7] G. Vidal, Efficient Classical Simulation of Slightly Entangled Quantum Computations, *Phys. Rev. Lett.* **91**, 147902 (2003).
- [8] F. Verstraete, D. Porras, and J. I. Cirac, DMRG and Periodic Boundary Conditions: A Quantum Information Perspective, *Phys. Rev. Lett.* **93**, 227205 (2004).
- [9] S. R. White, Density Matrix Formulation for Quantum Renormalization Groups, *Phys. Rev. Lett.* **69**, 2863 (1992).
- [10] J. Dukelsky, M. A. Martin-Delgado, T. Nishino, and G. Sierra, Equivalence of the variational matrix product method and the density matrix renormalization group applied to spin chains, *Europhys. Lett.* **43**, 457 (1998).
- [11] U. Schollwöck, The density-matrix renormalization group, *Rev. Mod. Phys.* **77**, 259 (2005).
- [12] F. Verstraete and J. I. Cirac, Renormalization algorithms for Quantum-Many Body Systems in two and higher dimensions, [arXiv:cond-mat/0407066](https://arxiv.org/abs/cond-mat/0407066).
- [13] G. Sierra and M. A. Martin-Delgado, *Proceedings of the Workshop on the Exact Renormalization Group, Faro, Portugal, 1998* (World Scientific, Singapore, 1998).
- [14] G. Vidal, Entanglement Renormalization, *Phys. Rev. Lett.* **99**, 220405 (2007).
- [15] V. Giovannetti, S. Montangero, and R. Fazio, Quantum MERA Channels, *Phys. Rev. Lett.* **101**, 180503 (2008).
- [16] R. N. C. Pfeifer, G. Evenbly, and G. Vidal, Entanglement renormalization, scale invariance, and quantum criticality, *Phys. Rev. A* **79**, 040301(R) (2009).
- [17] F. Pollmann, A. M. Turner, E. Berg, and M. Oshikawa, Entanglement spectrum of a topological phase in one dimension, *Phys. Rev. B* **81**, 064439 (2010).
- [18] X. Chen, Z.-C. Gu, and X.-G. Wen, Classification of gapped symmetric phases in one-dimensional spin systems, *Phys. Rev. B* **83**, 035107 (2011).
- [19] N. Schuch, D. Pérez-García, and I. Cirac, Classifying quantum phases using matrix product states and projected entangled pair states, *Phys. Rev. B* **84**, 165139 (2011).
- [20] B. Swingle, Entanglement renormalization and holography, *Phys. Rev. D* **86**, 065007 (2012).
- [21] J. I. Latorre and G. Sierra, Holographic codes, [arXiv:1502.06618](https://arxiv.org/abs/1502.06618).
- [22] F. Pastawski, B. Yoshida, D. Harlow, and J. Preskill, Holographic quantum error-correcting codes: toy models for the bulk/boundary correspondence, *J. High Energy Phys.* **06** (2015) 149.
- [23] J. Molina-Vilaplana, Information geometry of entanglement renormalization for free quantum fields, *J. High Energy Phys.* **09** (2015) 002.
- [24] M. Miyaji, T. Numasawa, N. Shiba, T. Takayanagi, and K. Watanabe, cMERA as Surface/State Correspondence in AdS/CFT, *Phys. Rev. Lett.* **115**, 171602 (2015)
- [25] P. Caputa, N. Kundu, M. Miyaji, T. Takayanagi, and K. Watanabe, Liouville action as path-integral complexity: from continuous tensor networks to AdS/CFT, *J. High Energy Phys.* **11** (2017) 097.
- [26] T. Nishino, Density matrix renormalization group method for 2D classical models, *J. Phys. Soc. Jpn.* **64**, 3598 (1995).
- [27] V. Murg, F. Verstraete, and J. I. Cirac, Efficient Evaluation of Partition Functions of Frustrated and Inhomogeneous Spin Systems, *Phys. Rev. Lett.* **95**, 057206 (2005).
- [28] M. Levin and C. P. Nave, Tensor Renormalization Group Approach to Two-Dimensional Classical Lattice Models, *Phys. Rev. Lett.* **99**, 120601 (2007).
- [29] L. P. Kadanoff, Scaling laws for Ising models near T_c , *Physics* **2**, 263 (1966).

- [30] K. G. Wilson, Group and critical phenomena. I. Renormalization group and the kadanoff scaling picture, *Phys. Rev. B* **4**, 3174 (1971).
- [31] Z.-C. Gu and X.-G. Wen, Tensor-entanglement-filtering renormalization approach and symmetry-protected topological order, *Phys. Rev. B* **80**, 155131 (2009).
- [32] G. Evenbly and G. Vidal, Tensor Network Renormalization, *Phys. Rev. Lett.* **115**, 180405 (2015).
- [33] G. Evenbly and G. Vidal, Tensor Network Renormalization Yields the Multi-Scale Entanglement Renormalization Ansatz, *Phys. Rev. Lett.* **115**, 200401 (2015).
- [34] F. Verstraete and J. I. Cirac, Continuous Matrix Product States for Quantum Fields, *Phys. Rev. Lett.* **104**, 190405 (2010).
- [35] J. Haegeman, T. J. Osborne, H. Verschelde, and F. Verstraete, Entanglement Renormalization for Quantum Fields in Real Space, *Phys. Rev. Lett.* **110**, 100402 (2013).
- [36] D. Jennings, C. Brockett, J. Haegeman, T. J. Osborne, and F. Verstraete, Continuum tensor network field states, path integral representations and spatial symmetries, *New J. Phys.* **17**, 063039 (2015).
- [37] A. Tilloy and J. I. Cirac, Continuous Tensor Network States for Quantum Fields, *Phys. Rev. X* **9**, 021040 (2019).
- [38] Q. Hu, A. Franco-Rubio, and G. Vidal, Continuous tensor network renormalization for quantum fields, [arXiv:1809.05176](https://arxiv.org/abs/1809.05176).
- [39] J. Cotlera, M. R. M. Mozaffar, A. Mollabashi, and A. Naseh, Renormalization group circuits for weakly interacting continuum field theories, *Fortsch. Phys.* **67**, 1900038 (2019).
- [40] Y. Shimizu, Tensor renormalization group approach to a lattice boson model, *Mod. Phys. Lett. A* **27**, 1250035 (2012).
- [41] P. Di Francesco, P. Mathieu, and D. Senechal, *Conformal Field Theory* (Springer, New York, 2012).
- [42] I. Affleck, Universal Term in the Free Energy at a Critical Point and the Conformal Anomaly, *Phys. Rev. Lett.* **56**, 746 (1986).
- [43] H. W. J. Blöte, J. L. Cardy, and M. P. Nightingale, Conformal Invariance, the Central Charge, and Universal Finite-Size Amplitudes at Criticality, *Phys. Rev. Lett.* **56**, 742 (1986).